Window function influence on phase error in phase-shifting algorithms

Joanna Schmit and Katherine Creath

We present five different eight-point phase-shifting algorithms, each with a different window function. The window function plays a crucial role in determining the phase (wavefront) because it significantly influences phase error. We begin with a simple eight-point algorithm that uses a rectangular window function. We then present alternative algorithms with triangular and bell-shaped window functions that were derived from a new error-reducing multiple-averaging technique. The algorithms with simple (rectangular and triangular) window functions show a large phase error, whereas the algorithms with bell-shaped window functions are considerably less sensitive to different phase-error sources. We demonstrate that the shape of the window function significantly influences phase error.

Key words: Phase-shifting interferometry, algorithms, phase-error analysis.

1. Introduction

The phase-shifting technique is a powerful tool for retrieving information about the phase (wavefront) encoded in a fringe pattern. The temporal phase-shifting technique[1,2] requires that at least three fringe patterns be captured sequentially in time by a CCD camera. Each fringe pattern (or frame, because the image is captured by the CCD camera) is shifted by the same amount of phase with respect to the previous one. Typically, the phase shift between frames equals $\pi/2$. The phase is then calculated locally at each pixel from different frames. We previously referred to this method as the n-frame method (n refers to the number of registered frames). A spatial phase-shifting[3] counterpart to the temporal phase-shifting technique also exists that requires only one fringe pattern with proper carrier frequency fringes introduced so that the phase shift between consecutive pixels is equivalent to the phase shift between frames. Analogous to the n-frame technique, we call this the n-point, method but it is also called the spatial carrier phase-shifting technique or direct-phase interferometry.[4]

Both techniques can employ the same algorithms; the difference, however, is that in the n-frame technique samples are taken from consecutive frames, whereas in the n-point technique samples are taken from consecutive pixels. The peak-to-valley (P–V) phase error, which can be attributed to a number of different sources such as phase-shift miscalibration or detector nonlinearity, is exactly the same for both techniques; however, the character of the error differs.[5] For example, the number of ripples in the phase error due to phase-shift miscalibration approximately equals twice the number of fringes in the interferogram. Thus in the n-frame technique only a few ripples are noticeable in the phase error because the fringes in the interferogram are typically nulled out in the n-frame technique. However, in the n-point technique many ripples occur in the phase error because of the large number of fringes introduced into the interferogram. The choice of algorithm used to calculate the phase greatly affects the kinds and magnitudes of the different error values and even the error characteristics (see, for example, Ref. 6).

Not only is the number of algorithms from which to choose fairly large, but the number of techniques used to derive these algorithms is also quite large. Initially, single algorithms were reported for a particular interferometric application; only later were whole techniques described for the derivation of specific algorithms. Today most of the algorithms assume a constant and known phase shift; there do exist techniques to derive algorithms for nonconstant but known phase shift or constant but unknown

The authors are with the Optical Sciences Center, University of Arizona, Tucson, Arizona 85721.

Received 3 August 1995; revised manuscript received 6 March 1996.

0003-6935/96/285642-08$10.00/0

phase shift, but these are not discussed here. Some popular, early techniques used the least-squares fit to a sinusoidal function proposed by Morgan.[7] Greivenkamp[8] presented a more general technique based on the least-squares fit, not necessarily deriving new algorithms but bringing together many existing methods. Womack[9] transferred a temporal technique to spatial interferometry, that emphasized the importance of the window function that the intensity is multiplied by. Larkin and Oreb[10] presented a technique for designing symmetrical algorithms based on a Fourier description of phase-shifting interferometry that was first presented by Freischald and Koliopoulos.[11] This elegant technique permits the derivation of algorithms that suppress a specific harmonic of the measured signal. Surrel[12] contributed a technique based on averaging the first and last interferogram to reduce phase error. The averaging technique introduced by Schwider[13] was the basis for our work in deriving many algorithms; following Schwider's lead, we called our technique the extended averaging technique.[14] The importance of the window function in reducing phase error was generally agreed on by many of the above authors, and we used the extended averaging technique to derive the window function values explicitly.[14] Recently de Groot[15] presented a technique in which the algorithms are derived by integer approximation to the analytical window function used in signal processing resulting in algorithms that were highly insensitive to sources of error. We emphasize the importance of the window function in phase-shifting interferometry by presenting and analyzing a few algorithms with different window functions but a constant number of samples, thereby confirming the influence of the window function on phase error.

To illustrate the influence of the window function on phase error we chose eight-point algorithms with different window functions and a $\pi/2$ phase shift. (For convenience, in this paper we refer to eight-*point* algorithms, even though these algorithms may be used in the n-frame technique as well.) The eight-point algorithms show (more so than algorithms with fewer intensity samples) the influence that the window function shape has on phase error. The five separate algorithms we constructed are characterized by their window functions, which are either rectangular, triangular, or bell shaped. The triangular and bell-shaped functions were derived based on a new error-reducing multiple-averaging technique that is related to the averaging[12] and extended averaging techniques.[14] All of these averaging techniques are presented in Section 2. In section 3 we present two equivalent sets of five eight-point algorithms, and in Section 4 we discuss the influence of the shapes of the window functions on phase error. Finally, Section 5 contains an analysis of phase error based on both computer simulation and real data. We show that not only does the number of samples determine how efficient an algorithm is, but that the choice of the sampling window also must be considered when selecting an appropriate error-reducing algorithm. The algorithm with a rectangular window function is the most sensitive to phase-shift miscalibration; the algorithms with bell-shaped window functions most effectively reduce the effects of phase-shift miscalibration.

2. Averaging Techniques

Phase-shifting techniques are based on the synchronous detection techniques introduced into optics from the telecommunications discipline by Bruning.[16] The general algorithm for calculating the phase $\varphi(x)$ of measured signal $I(x)$ in this technique can be represented as in Eq. (1):

$$\tan[\varphi(x_i)] = -\frac{\sum_{i=1}^{M} I_i(x_i)\sin\left(\frac{2\pi}{K}x_i + \theta\right)h(x_i)}{\sum_{i=1}^{M} I_i(x_i)\cos\left(\frac{2\pi}{K}x_i + \theta\right)h(x_i)}. \quad (1)$$

The measured signal $I(x)$ is multiplied by the reference signal (sine and cosine, respectively) and the window function, where the window function is designated as $h(x)$. The combination of the reference signal and the window function is the sampling function. M designates the number of measured intensity samples (either points or frames), $2\pi/K$ is the assumed phase shift between samples (also the sampling period), where K is an integer and θ is the initial phase. Note that the signal does not have to be sampled over just one period, as most algorithms assume; however, the sums of the sampling function values in the numerator as well as the denominator must equal zero.[10] A wise choice of reference signal frequency, sampling period, and initial phase will yield quite simple algorithms that are suitable for phase-shifting interferometry.

Phase-shifting algorithms can be derived by many different methods. For this article we review two of them, the averaging technique[13] and the extended averaging technique,[14] and present a new one, the multiple averaging technique. All of these techniques are closely related.

A. Conventional Averaging Technique

Any phase-shifting algorithm can be presented as

$$\tan\varphi = N/D, \quad (2)$$

where N and D are the numerator and the denominator of Eq. (1). In the averaging technique[13] two data sets taken with a $\pi/2$ shift in the initial phase are combined into a new phase algorithm [see Eq. (3a)].

B. Extended Averaging Technique

A sequential application of the averaging technique to each previously derived algorithm yields a new algorithm with reduced phase errors. This sequential application of the averaging technique we call the extended averaging technique.[14] The resulting algorithms are very simple in form if the technique is applied to algorithms with a $\pi/2$ phase shift between

intensity samples, because then the number of intensity samples for phase calculation increases only by one with each subsequent application of the technique. For example, if the averaging technique is applied twice and started with the M-point algorithm (designated Mp), we obtain M + 1- and then M + 2-point algorithms in the form

$$(M+1)p_\theta = Mp_\theta + Mp_{\theta+\pi/2} = \frac{N_1+N_2}{D_1+D_2} = \frac{N'}{D'}, \quad (3a)$$

$$\begin{aligned}(M+2)p_\theta &= (M+1)p_\theta + (M+1)p_{\theta+\pi/2} \\ &= \frac{N'+N''}{D'+D''} = \frac{N_1+2N_2+N_3}{D_1+2D_2+D_3}. \end{aligned} \quad (3b)$$

The θ designates an arbitrary initial phase in the reference signal of the algorithms, and the indices 1, 2, and 3 by numerators and denominators represent the first, second, and third sets of data.

This technique was used to derive five-point, six-point, and seven-point algorithms,[14] Eqs. (4b), (4c), and (4d), from the four-point algorithm, Eq. (4a), with the initial phase $\pi/4$ in the reference signal. The algorithms are given below:

$$4p_{\pi/4} = \frac{I_1+I_2-I_3-I_4}{I_1-I_2-I_3+I_4}, \quad (4a)$$

$$5p_{\pi/4} = \frac{I_1+2I_2-2I_3-2I_4+I_5}{I_1-2I_2-2I_3+2I_4+I_5} = 4p_{\pi/4} + 4p_{3\pi/4}, \quad (4b)$$

$$6p_{\pi/4} = \frac{I_1+3I_2-4I_3-4I_4+3I_5+I_6}{I_1-3I_2-4I_3+4I_4+3I_5-I_6} = 5p_{\pi/4} + 5p_{3\pi/4}, \quad (4c)$$

$$\begin{aligned}7p_{\pi/4} &= \frac{I_1+4I_2-7I_3-8I_4+7I_5+4I_6-I_7}{I_1-4I_2-7I_3+8I_4+7I_5-4I_6-I_7} \\ &= 6p_{\pi/4} + 6p_{3\pi/4}. \end{aligned} \quad (4d)$$

C. Multiple-Averaging Technique

The eight-point algorithms we present in this paper are derived from the above algorithms by a technique similar to the averaging technique, which we call the multiple-averaging technique. In this technique the algorithms are derived from averaging not two but three (or more) sets of algorithms for data sets shifted by $\pi/2$ as shown below:

$$\begin{aligned}(M+2)p_\theta &= Mp_\theta + Mp_{\theta+\pi/2} + Mp_{\theta+\pi} \\ &= \frac{N_1+N_2+N_3}{D_1+D_2+D_3} = \frac{N'}{D'}, \end{aligned} \quad (5a)$$

$$\begin{aligned}(M+3)p_\theta &= Mp_\theta + Mp_{\theta+\pi/2} + Mp_{\theta+\pi} + Mp_{\theta+3\pi/2} \\ &= \frac{N_1+N_2+N_3+N_4}{D_1+D_2+D_3+D_4} = \frac{N''}{D''}. \end{aligned} \quad (5b)$$

Note that the extended averaging technique results in algorithms that are less sensitive to phase-shift miscalibration than does the multiple-averaging technique, a fact that we demonstrate in next sections. However, for our purposes in this article the multiple-averaging technique enables us to derive eight-point algorithms with characteristic window functions to study the effects of the shape of window functions on the phase error.

3. Eight-Point Algorithms

The first example of the eight-point algorithm simply employs a rectangular window function of value 1, as do most of the common algorithms (for example, three- and four-point algorithms). The phase shift between pixels (frames) is assumed to be $\pi/2$, and the initial phase $\pi/4$. With the general synchronous detection algorithm given by Eq. (1) in which $N = 8$, we obtain the eight-point algorithm given in Eq. (6a), which is referred to here as the 8-RECT algorithm:

$$\text{8-RECT} = \frac{I_1+I_2-I_3-I_4+I_5+I_6-I_7-I_8}{I_1-I_2-I_3+I_4+I_5-I_6-I_7+I_8}. \quad (6a)$$

If the n-point technique is used, the indices refer to the number of consecutive pixels in each set of eight pixels; if the n-frame technique is used, the indices refer to the number of sequentially captured frames. Although this algorithm has no real application, since there are many other algorithms that require a smaller number of intensity samples and yield better results (for example, the Schwider–Hariharan[17,18] five-point algorithm), we show this window function shape as a point of reference for the other window function choices. All the other algorithms were derived based on the multiple-averaging technique described briefly in Section 2.

Our next two examples of algorithms employ triangular window functions. The first algorithm, the 8-TRI4 algorithm given in Eq. (6b), is the sum of five four-point algorithms as in Eq. (4a), with shifted initial phase; the second, the 8-TRI5 algorithm given in Eq. (6c), is the sum of four five-point algorithms as in Eq. (4b), with shifted initial phase:

$$\begin{aligned}\text{8-TRI4} &= \frac{I_1+2I_2-3I_3-4I_4+4I_5+3I_6-2I_7-I_8}{I_1-2I_2-3I_3+4I_4+4I_5-3I_6-2I_7+I_8} \\ &= 4p_{\pi/4} + 4p_{3\pi/4} + 4p_{5\pi/4} + 4p_{7\pi/4} + 4p_{9\pi/4}, \end{aligned} \quad (6b)$$

$$\begin{aligned}\text{8-TRI5} &= \frac{I_1+3I_2-5I_3-7I_4+7I_5+5I_6-3I_7-I_8}{I_1-3I_2-5I_3+7I_4+7I_5-5I_6-3I_7+I_8} \\ &= 5p_{\pi/4} + 5p_{3\pi/4} + 5p_{5\pi/4} + 5p_{7\pi/4}. \end{aligned} \quad (6c)$$

The window functions result in the following values

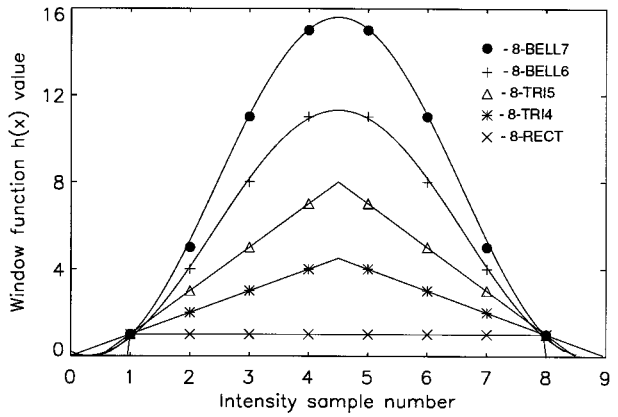

Fig. 1. Window function shapes.

at the sampling points [1, 2, 3, 4, 4, 3, 2, 1] and [1, 3, 5, 7, 7, 5, 3, 1], respectively. The values at the sampling points of these and other window functions presented in this paper are shown in Fig. 1.

The next two algorithms have bell-shaped window functions, the 8-BELL6 algorithm in Eq. (6d) and the 8-BELL7 algorithm in Eq. (6e):

$$\text{8-BELL6} = \frac{I_1 + 4I_2 - 8I_3 - 11I_4 + 11I_5 + 8I_6 - 4I_7 - I_8}{I_1 - 4I_2 - 8I_3 + 11I_4 + 11I_5 - 8I_6 - 4I_7 + I_8} = 6p_{\pi/4} + 6p_{3\pi/4} + 6p_{5\pi/4}, \tag{6d}$$

$$\text{8-BELL7} = \frac{I_1 + 5I_2 - 11I_3 - 15I_4 + 15I_5 + 11I_6 - 5I_7 - I_8}{I_1 - 5I_2 - 11I_3 + 15I_4 + 15I_5 - 11I_6 - 5I_7 + I_8} = 7p_{\pi/4} + 7p_{3\pi/4}. \tag{6e}$$

The values of the window functions equal [1, 4, 8, 11, 11, 8, 4, 1] and [1, 5, 11, 15, 15, 11, 5, 1], respectively, and are represented in Fig. 1. Worth noticing is that the 8-BELL7 algorithm [Eq. (6e)] belongs to the group of algorithms derived from the four-point algorithm [Eq. (4a)] by use of the extended averaging technique. Further application of this technique would yield algorithms of higher-number samples, i.e., 9, 10, and so on.

It is certainly possible to derive other eight-point algorithms in a similar way by using a different base algorithm, such as the one given below[19]:

$$4'p_0 = \frac{2(I_2 - I_3)}{I_1 - I_2 - I_3 + I_4}. \tag{7}$$

These algorithms would show an even smaller phase error due to phase-shift miscalibration; however, they would be more sensitive to the second harmonic in fringes, such as the second-order detector nonlinearity.[13] It is especially challenging to derive algorithms that are insensitive to one or more of the higher harmonics,[20] and they involve more complicated window functions.

The eight-point algorithms described by Eqs. (6a)–(6e) can be constructed in a much shorter form, giving exactly the same phase results and saving a bit of computational time, if they are derived from the four-point algorithm with an initial phase of 0 [Eq. (8)] instead of from the four-point algorithm with an initial phase of $\pi/4$ [Eq. (4a)]:

$$4p_0 = \frac{I_2 - I_4}{I_1 - I_3}. \tag{8}$$

The only difference between these shorter algorithms and the ones we presented above is in the initial phase of the reference sine and cosine signals. If the initial phase in the reference signals is $\pi/4$, then at each sampling point the cosine and sine functions take an absolute value of $\sqrt{2}/2$ (which is not visible in the algorithms because it cancels out in the numerator and denominator). If we choose an initial phase of zero, then every other intensity sample coefficient vanishes because at these points the sine or cosine equals zero.

Figure 2 presents the reference signals of the initial phase of 0 and $\pi/4$, clearly marking their values at the sampling points. Even though it appears that every other value of the window functions vanishes for the reference signals with initial phase 0, the window functions for both the shorter form and the longer form presented above are the same (see Fig. 1). The longer versions of the algorithms were constructed simply to show in the clearest way the shape of the window functions. What follows below are these shorter forms of the

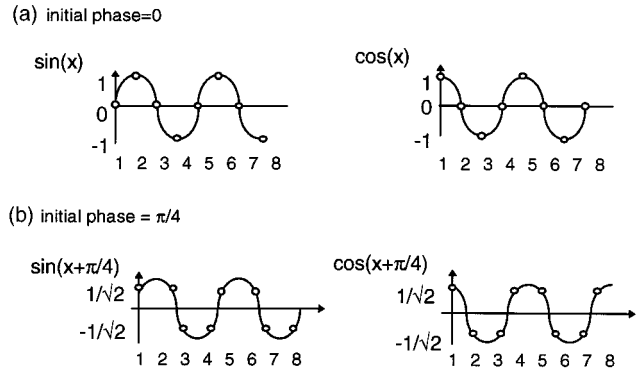

Fig. 2. Values of the reference signals (designated by circles) at the sampling points for reference signals with initial phases equal to 0 and $\pi/4$. The corresponding sample numbers are given below each reference signal.

eight-point algorithms:

$$\text{8-RECT}' = \frac{I_2 - I_4 + I_6 - I_8}{I_1 - I_3 + I_5 - I_7}, \tag{9a}$$

$$\text{8-TRI4}' = \frac{2I_2 - 4I_4 + 3I_6 - I_8}{I_1 - 3I_3 + 4I_5 - 2I_7} = 4p_0 + 4p_{\pi/2} + 4p_{\pi} + 4p_{3\pi/2} + 4p_0, \tag{9b}$$

$$\text{8-TRI5}' = \frac{3I_2 - 7I_4 + 5I_6 - I_8}{I_1 - 7I_3 + 5I_5 - 3I_7} = 5p_0 + 5p_{\pi/2} + 5p_{\pi} + 5p_{3\pi/2}, \tag{9c}$$

$$\text{8-BELL6}' = \frac{4I_2 - 11I_4 + 8I_6 - I_8}{I_1 - 8I_3 + 11I_5 - 4I_7} = 6p_0 + 6p_{\pi/2} + 6p_{\pi}, \tag{9d}$$

$$\text{8-BELL7}' = \frac{5I_2 - 15I_4 + 11I_6 - I_8}{I_1 - 11I_3 + 15I_5 - 5I_7} = 7p_0 + 7p_{\pi/2}. \tag{9e}$$

The 8-BELL7′ algorithm was derived in the same way as the algorithm in Eq. (6e), namely, from the average of two seven-point algorithms, but with initial phase 0. This seven-point algorithm was also presented by de Groot and Deck.[21] The window function in 8-BELL7 algorithms [Eq. (6e) and (9e)] is an approximation to the Hanning window as it was shown by de Groot.[15]

4. Window Functions

From a mathematical point of view, the convolution in the space domain of the measured quasi-sinusoidal signal with the reference sine and cosine signals can be thought of as the Fourier transform of the measured signal. The popular fast Fourier transform (FFT) technique introduced by Takeda[22] uses the Fourier transformation of the measured signal and filters the spectrum to find the phase. Both the n-point and the FFT techniques usually require only one fringe pattern with carrier frequency fringes introduced; however, the n-point technique operates in the space domain and the FFT works in the spectrum domain of the fringe pattern. In both techniques the fringe pattern is not an unlimited quasi-sinusoidal signal; the truncation of the signal results in the convolution of the unlimited signal spectrum with the truncating function spectrum. The truncating function is referred to as the window function in this paper. This convolution widens the spectrum of sinusoidal signals and may introduce additional high-frequency components (the leakage problem). The Fourier transform technique uses a wide window function that is limited only by the size of the CCD array or the aperture of the fringe pattern (see Fig. 3). In contrast, the n-point technique uses a window function equivalent in width to a few pixels or, specifically in our case, to eight pixels. As the width of the rectangular window function increases, its spectrum narrows and the measured signal spectrum is represented more accurately. Therefore, the Fourier transform technique may result in a higher level of accuracy[4,23] in the center of the interferogram than the n-point technique, and this technique may be useful in testing elements in which the outer area of an element does not play an important role during use. The large phase errors found at the edges of interferograms in the FFT technique are related to the Gibbs phenomena at the discontinuities of the tested signal.[23] However, the advantage of the n-point technique can be its fairly uniform phase error over the entire area of the interferogram, which avoids the large phase errors at the edges and can be important in testing elements up to their edges. Another advantage of the n-point technique is its relatively short computational time, which makes it especially attractive for real-time applications.

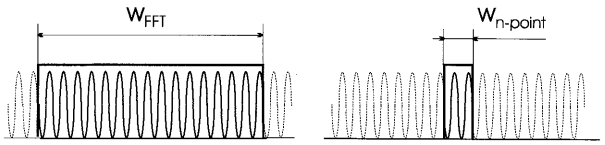

Fig. 3. Intensity signal truncated by the rectangular window functions in FFT and n-point techniques.

Because the phase error depends on the characteristics of the window function spectrum, the usual technique is to introduce the apodization in a window function. The Hamming or Hanning apodizations are the most popular in the FFT technique.[24,25] They significantly change the shape of the window function, and their spectrum has a relatively narrow major lobe and low side lobes. Similar apodizations of the window function should certainly reduce the errors in the n-point technique. The subject of the importance of the window function in phase-shifting algorithms has been raised previously.[9–11] Some of the algorithms with explicitly given values of error-reducing window functions were presented in our previous work.[14] Recently de Groot[15] presented a method for deriving new algorithms from an integer approximation of analytical window functions used in signal processing. The examples he used varied not only in the shape of the window function but also in the number of intensity samples. Because it is known that a larger number of intensity samples very often results in a smaller phase error, the specific influence of the window function could not be isolated as the only factor in reducing the phase error. By keeping the number of samples constant and simply changing the window function, it is possible to avoid this ambiguity and thus document the importance of the shape of the window function. Thus in this paper we provide the algorithms for the same number of samples, but with different window functions, and analyze some of their errors.

We now look at the Fourier spectrum of the measured signal for two eight-point algorithms. The measured sinusoidal signals are truncated, the first by the rectangular window function (8-RECT) and

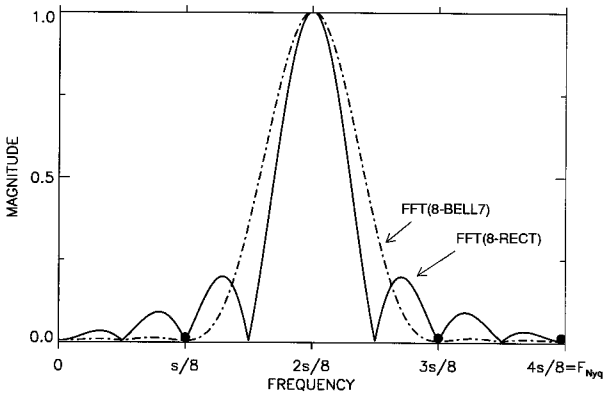

Fig. 4. Fourier spectra of signals multiplied by the 8-RECT and 8-BELL7 window functions, shown only for positive frequencies up to the Nyquist frequency. Signals are sampled with spacing s. The period of the measured sinusoidal signal equals $4s$, and the width of the window equals $8s$. Dots represent sampling points in each spectrum.

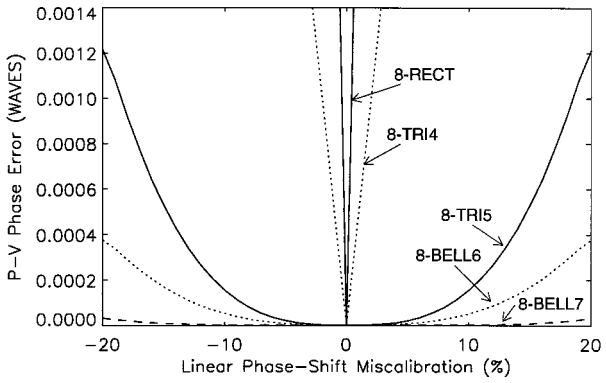

Fig. 5. P–V phase error versus percent of phase-shift miscalibration.

the second by the Hanning window function (8-BELL7). Signals are sampled at eight points with spatial spacing s. Two full periods of sinusoidal signal are enclosed within the window function, giving an exact $\pi/2$ change in phase from point to point as assumed in the algorithms. The Fourier spectra of those two modified signals, shown in Fig. 4, result in the convolution of the window function spectra with two delta functions at the frequency of the input sinusoidal signal. Because of the discrete sampling of the input signal, the spectrum is also calculated at discrete points, designated dots. When the ideal phase change $\pi/2$ between pixels is introduced, the spectrum consists of a single pair of delta functions at the frequency of the input signal (because the rest of the values at the discrete points of the spectrum are at the zeros of the window function spectra). Thus a discrete spectrum perfectly represents an unlimited input signal spectrum. However, when the phase change between pixels is something other than $\pi/2$, the frequency of the measured signal changes, and no longer are there two complete cycles of signal within a window. In the spectrum domain the two lobes (one in the positive and the other in the negative frequency domain) are shifted with respect to the discrete points of the spectrum domain, thereby introducing some higher-order harmonics to the main harmonic of the signal. The spectrum of the Hanning window has smaller side lobes than the spectrum of the rectangular window function; thus the magnitude of unwanted higher-order harmonics will be smaller. The small side lobes in the spectrum are more important than its narrow main lobe because a continuously changing phase from point to point, which is inherent in the n-point method, will always introduce higher harmonics.

In Section 5 we analyze the sensitivity of the eight-point algorithms to phase-shift miscalibration in computer simulation and show that algorithms with bell-like window functions (i.e., the Hanning function) are the least sensitive to phase-shift miscalibration. The influence of the window function shape on phase error could be investigated in other ways, for example, either by computer simulation[6,14] or a Fourier analysis of sampling functions.[10,11,14] However, regardless of the method, the same conclusions about the algorithms' sensitivities to different error sources would be reached.

5. Phase Errors

In Fig. 5 we present a diagram of the P–V error due to linear phase-shift miscalibration, which is the most common error source in phase-shifting interferometry. The 8-RECT algorithm is really the sum of two four-point algorithms shifted in phase by 2π; thus it results in the same phase-error values as the common four-point algorithm for linear phase-shift miscalibration. These errors are very large when compared with any eight-point algorithm with a bell-shaped window function. The 8-BELL6 and 8-BELL7 algorithms are all less sensitive to phase-shift miscalibration than is the Schwider–Hariharan[17,18] five-point algorithm. The 8-BELL7 algorithm is the least sensitive of all of the eight-point algorithms, which indicates that the extended averaging technique is a better way to derive error-reducing algorithms than a multiple-averaging technique. For a phase-shift miscalibration of 20%, the P–V phase error equals only 0.00003 of the wavelength when the 8-BELL7 algorithm is used as shown in Fig. 5. An error of this small scale is hardly comparable with the magnitude of the phase error due to the noise encoded in the fringe pattern. Figure 6 represents the phase errors for the three least sensitive eight-point (not eight-frame) algorithms. The errors are due to phase-shift miscalibration by 6.25%, which is equivalent to a 2-fringe tilt miscalibration per 128 pixels.

Figure 7 shows the phase retrieved from the real interferogram with 8-RECT and 8-BELL7 algorithms. The algorithm with the rectangular window function produces a phase with clearly noticeable ripples owing to a phase-shifter miscalibration, but in the phase produced by the algorithm with the bell-like window function the ripples are not noticeable

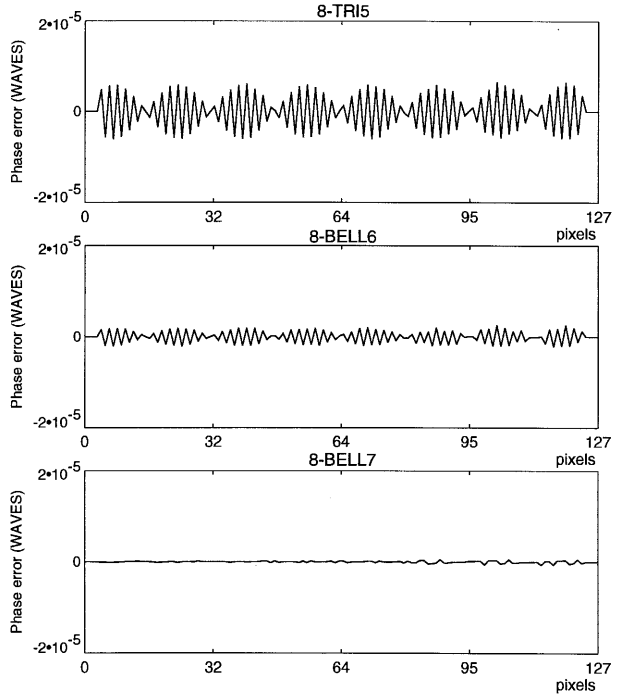

Fig. 6. Phase errors for three eight-point algorithms, due to 6.25% phase-shift miscalibration (2-fringe tilt miscalibration).

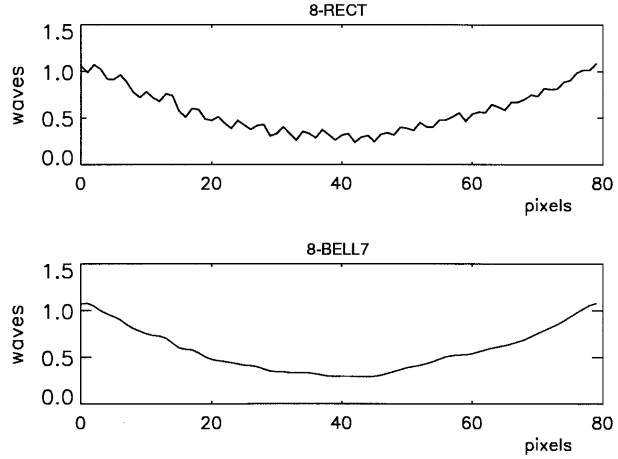

Fig. 7. Phase retrieved from real data with 8-RECT and 8-BELL7 algorithms.

because they blend in with the errors due to some kind of noise in the interferogram. If the main source of error is noise in the interferogram, then no regular ripples are noticeable; however, even then the error in phase is reduced when the 8-BELL7 algorithm is used. When severe phase-shift miscalibration occurs (owing to any error source), the phase error may be so significant that the phase unwrapping procedure may fail if a poor error-reducing algorithm is used for phase calculation.

6. Conclusions

We presented five eight-point algorithms that differ only in the shape of their window function. The algorithms that use either a rectangular or a triangular window function result in large phase errors while the algorithms with bell-shaped window functions are quite insensitive to phase-shift miscalibration. The shape of the window function in the n-point algorithms plays an important role in reducing phase error. The algorithm called 8-BELL7 shows the smallest sensitivity to different error sources. This algorithm was derived by use of the extended averaging technique,[14] which indicates that this technique is an excellent method for constructing an error-compensating algorithm. The compensation for phase-shift miscalibration or other nonlinear errors could be performed by first measuring the phase shift at each point and then introducing the measured phase shift into an algorithm in an iterative way[26]; however, this method seems to be quite time consuming. The importance of our algorithms lies in their high insensitivity to phase-shift miscalibration along with efficient computation. This insensitivity is a significant factor in interferometers with Fizeau cavities in which the phase shift varies with the distance away from the axis.[27–29]

References and Notes

1. K. Creath, "Temporal phase measurement methods," in *Interferogram Analysis: Digital Fringe Pattern Measurement Technique*, D. W. Robinson and G. T. Reid, eds. (Institute of Physics, Bristol, U.K., 1993), Chap. 4, pp. 94–140.
2. J. E. Greivenkamp and J. H. Bruning, "Phase shifting interferometers," in *Optical Shop Testing*, 2nd ed., D. Malacara, ed. (Wiley, New York, 1992), Chap. 14.
3. See, for example, M. Kujawinska, "Spatial phase measurement methods," in *Interferogram Analysis: Digital Fringe Pattern Measurement Technique*, D. W. Robinson and G. T. Reid, eds. (Institute of Physics, Bristol, U.K., 1993), Chap. 5, pp. 141–193.
4. D. Malacara and S. L. DeVore, "Direct measuring interferometry," in *Interferogram Analysis: Digital Fringe Pattern Measurement Technique*, D. W. Robinson and G. T. Reid, eds. (Institute of Physics, Bristol, U.K., 1993), Chap. 13.6, pp. 494–500, and references within.
5. J. Schmit, K. Creath, and M. Kujawinska, "Spatial and temporal phase-measurement techniques: a comparison of major error sources in one-dimension," in *Interferometry: Techniques and Analysis*, G. M. Brown, M. Kujawinska, O. Y. Kwon, and G. T. Reid, eds., Proc. SPIE **1755,** 202–211 (1992).
6. K. Creath and J. Schmit, "*N*-point spatial phase measurement techniques for nondestructive testing," Opt. Lasers Eng. **24,** 365–379 (1996).
7. C. J. Morgan, "Least-squares estimation in phase-measurement interferometry," Opt. Lett. **7,** 368–373 (1982).
8. J. E. Greivenkamp, "Generalized data reduction for heterodyne interferometry," Opt. Eng. **23,** 350–352 (1984).
9. K. H. Womack, "Interferometric phase measurement using spatial synchronous detection," Opt. Eng. **23,** 391–395 (1984).
10. K. G. Larkin and B. F. Oreb, "Design and assessment of symmetrical phase-shifting algorithms," J. Opt. Soc. Am. A **9,** 1740–1748 (1992).
11. K. Freischald and C. Koliopoulos, "Fourier description of digital phase-measuring interferometry," J. Opt. Soc. Am. A **7,** 542–551 (1990).
12. Y. Surrel, "Phase stepping: a new self-calibrating algorithm," Appl. Opt. **32,** 3598–3600 (1993).
13. J. Schwider, "Advanced evaluation techniques in interferom-

etry," in *Progress in Optics XXVIII*, E. Wolf, ed. (Elsevier, New York, 1990), Chap. 4, pp. 271–359.
14. J. Schmit and K. Creath, "Extended averaging technique for derivation of error-compensating algorithms in phase shifting interferometry," Appl. Opt. **34,** 3610–3619 (1995).
15. P. de Groot, "Derivation of algorithms for phase-shifting interferometry using the concept of a data sampling window," Appl. Opt. **34,** 4723–4730 (1995).
16. J. Bruning, D. H. Herriot, J. E. Gallagher, D. P. Rosenfeld, A. D. White, and D. J. Brangccio, "Digital wavefront measuring interferometer for testing optical surfaces and lenses," Appl. Opt. **13,** 2693–2703 (1974).
17. J. Schwider, R. Burow, K. E. Elsner, J. Grzanna, R. Spolaczyk, and K. Merkel, "Digital wave-front measuring interferometry: some systematic error sources," Appl. Opt. **22,** 3421–3432 (1983).
18. P. Hariharan, B. F. Oreb, and T. Eiju, "Digital phase-shifting interferometry: a simple error-compensating phase calculation algorithm," Appl. Opt. **26,** 2504–2505 (1987).
19. J. Schwider, O. Falkenstorfer, H. Screiber, A. Zoller, and N. Streibl, "New compensating four-phase algorithm for phase-shift interferometry," Opt. Eng. **32,** 1883–1885 (1993).
20. K. Hibino, B. F. Oreb, D. I. Farrant, and K. G. Larkin, "Phase shifting for nonsinusoidal waveforms with phase-shift errors," J. Opt. Soc. Am. A. **12,** 761–768 (1995).
21. P. de Groot and L. Deck, "Long-wavelength laser diode interferometer for surface flatness measurement," in *Optical Measurements and Sensors for the Process Industries*, C. Gorecki and R. W. Preater, eds., Proc. SPIE **2248,** 136–140 (1994).
22. M. Takeda, "Spatial carrier fringe pattern analysis and its application to precision interferometry: an overview," Ind. Met. **1,** 79–99 (1990).
23. M. Kujawinska and J. Wojciak, "High accuracy fourier transform fringe pattern analysis," Opt. Lasers Eng. **14,** 325–339 (1991).
24. R. W. Ramirez, *The FFT: Fundamentals and Concepts* (Prentice-Hall, Englewood Cliffs, N.J., 1985).
25. A. A. Malcolm, D. R. Burton, and M. J. A. Lalor, "A study of the effect of windowing on the accuracy of surface measurements obtained from the Fourier analysis of fringe pattern," in *Proceedings of FASIG Fringe Analysis '89*, *Loughborough University of Technology*, *4–5 April 1989* (The Fringe Analysis Special Interest Group, 1989).
26. C. Joenathan, "Phase-measuring interferometry: new methods and error analysis," Appl. Opt. **33,** 4147–4155 (1994).
27. P. de Groot, "Phase-shift calibration errors in interferometers with spherical Fizeau cavities," Appl. Opt. **34,** 2856–2863 (1995).
28. R. C. Moore and F. H. Slaymaker, "Direct measurement of phase in a spherical-wave Fizeau interferometer," Appl. Opt. **19,** 2196–2200 (1980).
29. K. Creath and P. Hariharan, "Phase-shifting errors in interferometric tests with high-numerical-aperture reference surfaces," Appl. Opt. **33,** 24–25 (1994).